

# The Roll Effect in Erupting Prominences

Patrick D. Bangert<sup>1</sup>, Sara F. Martin<sup>2</sup>, Mitchell A. Berger<sup>3</sup>

## Abstract

From observations it is known that many filaments have the overall structure of long thin sheets of mass that we will refer to as a ribbon. Based on counter-streaming mass flows observed in filaments, we assume that the filaments have internal magnetic fields (thermally isolated from the surrounding coronal fields) that are aligned with the ribbon. We then use the ribbon hypothesis to explain an observable effect which we term the *roll effect*. Briefly, the nature of the roll effect is manifested by a filament ribbon in its slow pre-eruptive rise through the tendency to be non-radial, with a small preferential roll in one direction. When it erupts and further rises, the most elevated portion bends over in the roll direction and is forced to become nearly horizontal. Propagation of the roll down the legs of the filament twists them in opposite directions consistent with Doppler motions in a few observed examples. Each of the two primary directions of roll have a one-to-one correspondence with the two forms of filament chirality. Because the rolling can occur in only two possible forms of handedness, it constitutes an observable form of chirality specific to erupting filaments. We give a theoretical explanation of this effect which leads us to predict that the filaments that exhibit the roll effect are not centered beneath the overlying arcade of coronal magnetic fields (the verification of this effect is the subject of future work).

## 1 Introduction

The nature and structure of the magnetic fields of filaments (prominences) has received broad speculation and has been the subject of extensive modelling. Because we still lack complete observational information on their magnetic field topology, models have been based on various assumptions on how the mass of filaments is related to coronal magnetic fields. Currently filaments are often treated as mass embedded in the lowest part of a magnetic flux tube in the corona [8, 22, 2]. A common assumption in the research on filaments is that flux tubes are of circular or near-circular cross-section (see for instance [18, 4] and figure 1 (a)). Alternatives to flux tube models have been proposed also. A few models have the common property of consisting of sets of loops that are aligned or nearly aligned with the long axis of the filament [1, 11]. In these models, the filament has its own magnetic field separate from the surrounding coronal magnetic fields and separately rooted in the photosphere from the coronal magnetic fields which overly all filaments. A cross-section representative of

---

<sup>1</sup>International University Bremen, P.O. Box 750 561, 28725 Bremen, Germany, [p.bangert@iu-bremen.de](mailto:p.bangert@iu-bremen.de)

<sup>2</sup>Helio Research Inc., 5212 Maryland Ave., La Crescenta, CA 91214, USA, [sara@oxygen.helioresearch.org](mailto:sara@oxygen.helioresearch.org)

<sup>3</sup>University College London, Gower Street, London WC1E 6BT, United Kingdom, [m.berger@ucl.ac.uk](mailto:m.berger@ucl.ac.uk)

these models is shown in figure 1 (b) for active region filaments and 1 (c) for quiescent filaments.

In this paper we view filaments as in the alternate model 1 (b). The only differences between figures 1 (b) and 1 (c) are the heights of the filament mass above the chromosphere and the representation of the barbs. The barbs are threads or groups of threads that branch from the axis of the filament to the chromosphere on each side of the filament and are not relevant to the initial stages of this model. The justification for using this model comes from the observation of filaments such as those discussed and illustrated in section 2. The ribbon has one edge lying on the chromosphere and the other edge vertically above in the corona as in figure 2. Its primary magnetic field runs the full length of the ribbon and is assumed to connect to the active region or network magnetic fields at its extreme ends.

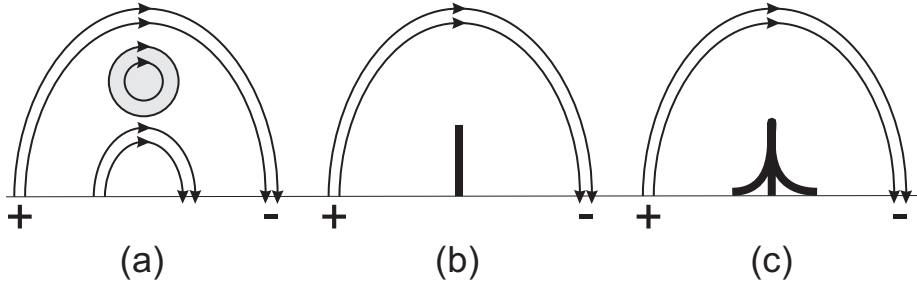


Figure 1: In figure (a) we see the twisted prominence model in which the filament has a roughly circular cross section [4]. Based on observations, we believe that the vast majority of active region filaments are thin sheets of mass like a ribbon seen in cross section as in (b). The quiescent filaments have additional sheets that extend from the main sheet to specific minor polarity boundaries at the photosphere seen in cross section as in (c).

As we illustrate during symmetric eruptions, a ribbon develops one of two patterns and these two patterns have a one-to-one relationship to filament chirality. The two patterns are mirror images of each other and are uniquely related to the magnetic field directions along the axis of the filament and the inferred coronal field around the filament. As such these patterns constitute handedness and thus are newly recognized forms of chirality. We find evidence of this form of dynamic chirality in erupting prominences in published spectra, in He II 304Å images from EIT/SOHO, in some TRACE series of images and in some H $\alpha$  time-lapse sequences of images. In this paper we describe and define the phases of this form of dynamic chirality and call it the “roll effect.”

Our concern in this paper is how filament chirality is observed when a filament erupts. Depending upon filament magnetic field models conceived to date, the expectation has been that dextral filaments will either reveal right-hand twist as anticipated by [13] or left-hand twist as anticipated by [21] consistent

with flux-tube models such as those of [8, 20, 22]. Observations of twist in erupting filaments are very common. However, the debate on which association is correct has remained because in most observations it is not possible to determine unambiguously whether the twist is right-handed or left-handed. To determine this, one needs information on the topology of erupting filaments, or at the very least, key information on the spatial dimension in the line of sight; for structures which appear to cross in the line-of-sight, one needs to know without ambiguity which is in front and which is in back as illustrated by [5].

In section 2, we illustrate the ribbon-like structure of filaments. In section 3, we define filament and arcade chirality. In section 4, we illustrate the nature of the roll effect, namely that a pre-eruptive filament begins to roll in a preferential direction and secondly that an eruptive filament ribbon rolls over so that its initially vertical cross-section becomes horizontal, and in section 5 we explain the roll effect by means of theoretical model which, if it is going to explain the roll effect, makes an additional prediction of a translational skew of the arcade which has yet to be verified by experiment. We give observational evidence of the roll effect in section 6, discuss our results in section 7 and conclude in section 8.

## 2 Observations of the Ribbon Structure of Filaments

The ribbon structure can be thought of as a stack of horizontal threads, one above the other and having a total apparent width of about one or two threads and a height of 5 to 50 threads; the height can vary several factors along the length of a filament such that the threads have variable density or spacing in the vertical direction. The length can vary greatly but typically the length is tens to hundreds of times the filament height. The lengths of filaments are thus commonly one to three orders of magnitude greater than their width and thus have a ribbon-like structure along the majority of their length.

Large active region filaments are the ones that most clearly resemble ribbons. An example is illustrated in figure 2. The true width of the ribbon in figure 2 can be estimated at the point where the filament has a bend. The bend, and orientation of the filament with respect to the observer, allows one to see part of one side of the filament beyond the bend and to view the other side of the filament on the near side of the bend. At the bend one sees neither side better than the other. Hence the width of the filament at the bend is the maximum width of the narrowest dimension of the filament. The example in figure 2 is a maximum of 3000 km wide at the bend, approximately 20,000 km high if the filament ribbon is vertical and a minimum of 390,000 km long.

Due to the sun's rotation, filaments appear to transit the solar disk throughout their lifetimes that may vary from a few hours to a few weeks. For those with lifetimes of a few days or more, this affords many opportunities to observe them from different perspectives and thereby deduce some features of

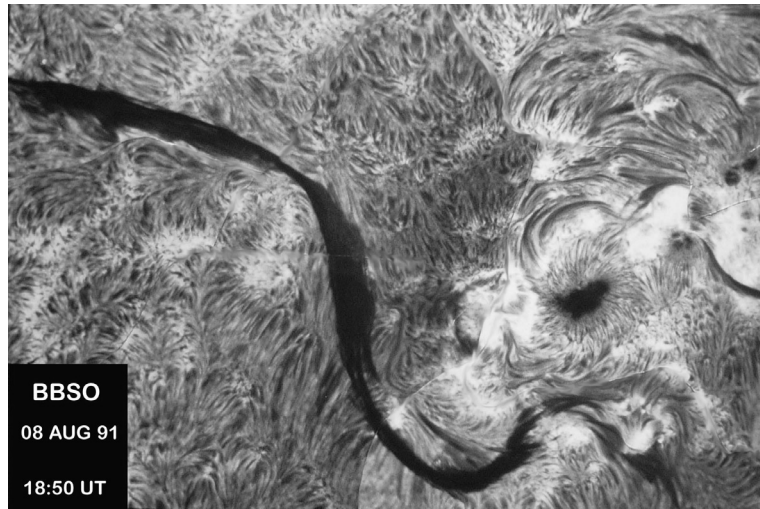


Figure 2: Ribbon-like filament 31 Aug. 1991, Big Bear Solar Observatory. Large active region filaments like this one most closely resemble ribbons with a width of 3000 km, height of 20,000 km and length of 390,000 km.

their overall topology. Commonly we see filaments broadside (i.e. their axis is near-perpendicular to the viewing direction). However, some filaments, within or near the active region belt in the northern hemisphere, have a north-east to south-west orientation which is nearly linear. Similarly, some filaments in the southern hemisphere have a south-east to north-west orientation. Near the east limb, this allows one to look down and along the axis of a filament for an appreciable distance of its length. Such views for quiescent filaments also show that the top of the long axis of these filaments is also very narrow. Characteristically the axial component is only a few arc seconds wide. For quiescent filaments, additional width is provided only by the barbs that extend from the axis to the chromosphere on both sides of the filament as shown in figure 3.

Figure 3 (Sept. 12-15, 2002) is an example observed at Helio Research of a typical long, tall and narrow quiescent filament as it appears to cross the limb and come onto the solar disk due to solar rotation. At the limb the filament was seen to have a minimum height of 62,000 km at its highest point above the limb on the 12<sup>th</sup> of September; this is a lower limit to its true height. Thereafter, the apparent height (the distance from the top of the filament to the chromosphere) decreases. As the Sun rotates, the filament is gradually revealed as a dark structure against the solar disk and the distance from its top to the polarity boundary below gradually continues to decrease. The south edge is very sharp and defines the top of the filament in H $\alpha$ . The irregular north reveals the barbs. This edge is the lowest part of the filament where the barbs intersect the chromosphere. Gradually from the 12<sup>th</sup> to the 14<sup>th</sup>, the

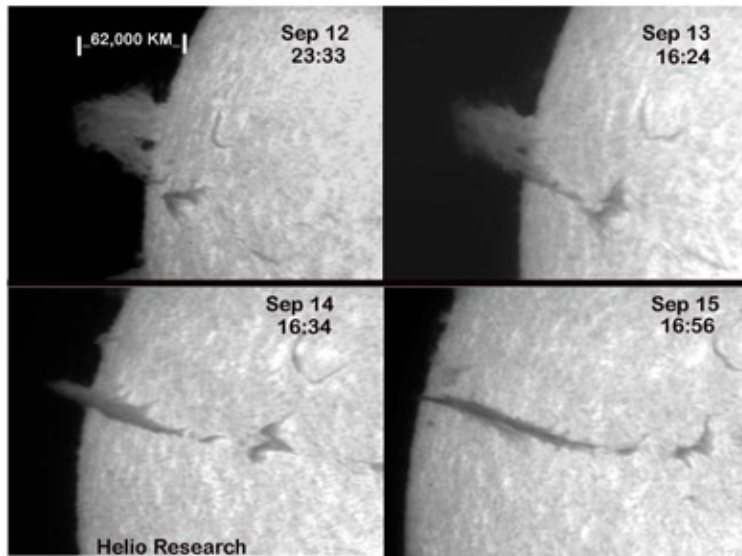


Figure 3: Ribbon-like filament on 2002 Sep. 15. This is an example of a quiescent filament closely resembling a ribbon with a width of 3500 km, height of 62,000 km and length of 450,000 km.

irregular north side becomes more narrow and by the 15<sup>th</sup> the barbs on the south side become visible. In sections along the axis where the sets of barbs are approximately equal in length on each side, we are viewing the filament from above and along the axis. Near the limb is a section where there are no barbs and we are seeing the maximum width of the filament axis; at this location, the maximum width is 3500 km. Thus excluding the width due to the barbs out to 32,000 km, we see that the axis of this filament is not more than 3500 km wide, a minimum of 62,000 km high when crossing the limb and a minimum of 450,000 km long. With these relative dimensions, it is well described as having ribbon-like structure.

### 3 Filament Chirality

Filaments have a property termed *chirality* which comes in two flavors: *dextral* and *sinistral*. This property is intimately linked to the unique location of filaments over polarity reversal boundaries in between adjacent large regions of opposite magnetic field polarity. Such boundaries, called polarity inversion lines, are relatively distinct in magnetograms of the line-of-sight component of photospheric or chromospheric magnetic flux.

Suppose we are located on the positive polarity side of the photospheric polarity boundary line over which a filament resides. The *dextral* filament's

field lines point to the right and the *sinistral* filament’s field lines point to the left (see figure 4). A number of other aspects of chirality may be found in [14, 16]. Dextral filaments predominate in the northern hemisphere and sinistral filaments in the southern hemisphere [14, 10]. Note also that the sign of magnetic field polarity (and hence the direction of the arrows) is a convention and can thus be changed *but* that the definition of chiralities is invariant under this change.

Each filament comes with an overlying system of coronal loops, the composite of which is known as the “coronal arcade.” It is now a common observation from X-ray and EUV images that this arcade structure is skewed, i.e. that the arcade structure is not perpendicular to the filament. The arcade is *right-skewed* if the acute angle is on the right-hand, near side of the observer located on the positive polarity side of the polarity boundary and *left-skewed* otherwise. There exists a one-to-one correspondence between chirality and skew [12]; right-skewed arcades reside over sinistral filaments and left-skewed arcades over dextral filaments (see figure 4). This skew is very important to our theoretical model that predicts a one-to-one correspondence between chirality and roll direction.

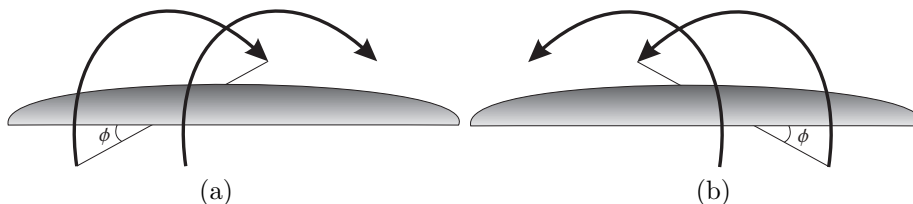


Figure 4: The shaded sheet represents a filament and the arcs represent the overlying arcade field. The two different chiralities for a filament ribbon are: (a) dextral with left-skewed arcade field and (b) sinistral with right-skewed arcade field. The angle  $\phi$  is defined by the diagram and will be used in our theoretical model. Note that, by definition,  $0 \leq \phi \leq 90$ .

## 4 Roll Effect Definition

In examples of erupting filaments that we have collected, we find evidence of the existence of a previously unrecognized form of chirality. This chirality is inherent in the sense of twist in the topology of the eruption and therefore gives us essential information on the 3-dimensional structure of some classic examples of erupting filaments. We call this dynamic form of chirality the *roll effect*.

See figure 5 for a stage-by-stage depiction of the initial roll effect of a filament ribbon. To picture how this may look in a real observation, see the comparison figure 6. We give the example of a nearly symmetric eruption in which the barbs (if any) detach from the chromosphere while the extreme ends of the filament remain anchored to the chromosphere/photosphere as illustrated in figures 2 and

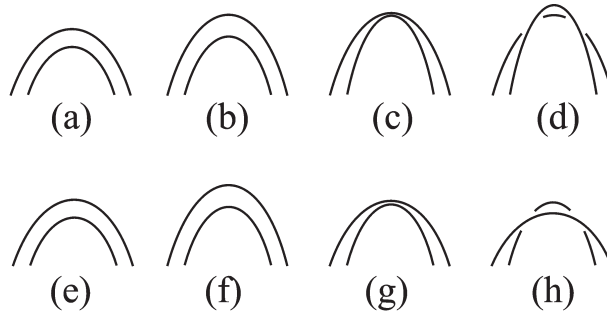


Figure 5: The observed roll effect for sinistral filaments is shown in (a) to (d) and for dextral filaments in (e) through (h). The diagram is to be understood as observed from the positive polarity side of the filament.

3. Prior to eruption, the ribbon has a vertical, narrow cross-section. During the early eruptive stage, the ribbon rises but experiences a containment force from the overlying arcade. Thus the lower parts of the filament rise faster than the top and the cross-section of the most elevated portion of the ribbon begins to roll-over and eventually approaches the horizontal. See figure 5 (a) to (d) for a depiction of the sinistral case and (e) to (h) for the dextral case. The initial state is displayed in (a) and (e), the filament ribbon then rises in (b) and (f), containment acts in (c) and (g) causing the roll in (d) and (h). Note that, as before, the observer in figure 5 is assumed to be on the positive polarity side of the boundary. The roll effect could also originate from a foot-point twisting motion as opposed to originating from the filament interaction with the arcade field; see figure 7. As discussed later, this alternative is however inconsistent with the Doppler observations presented in figure 12 (as well as examples 1 and 5 in table 1) and we conclude that the roll effect occurs as depicted in figure 5.

We define the two chiral forms of the roll effect in relation to the magnetic field direction of the coronal magnetic fields that are known to arch high over filaments from their dominantly positive to dominantly negative photospheric sides. The roll direction from the top of the filament in common with the component of magnetic field above is defined as “positive” roll and roll in the opposing direction to this magnetic field component is defined as “negative.”

The same two forms of rolling-over can be achieved if the endpoints (or more correctly for filament ribbons, *end line segments*) are turned both outwards (dextral, see figure 7 left) or both inwards (sinistral, see figure 7 right). We can distinguish between these two possibilities by examples in which Doppler shifts are observed within prominences; please see figure 12 for an example to be discussed later. If the roll originates as a twist of the foot-points, the roll propagates upwards into the filament. Conversely, if the roll originates at the top of the filament, the roll propagates downward to the foot-points.

It has been observed by [6, 3, 7] that such turning occurs at the chromo-

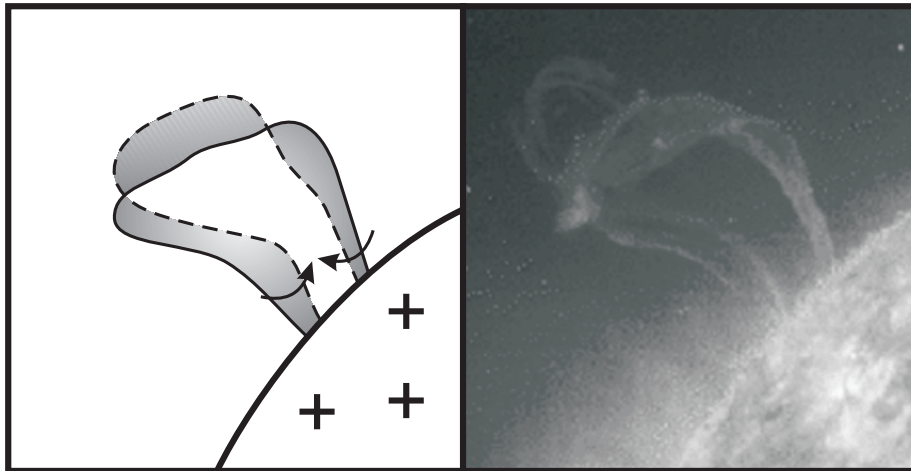


Figure 6: A section of figure 5 compared against an observation of March 6, 1999.

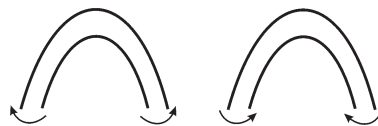


Figure 7: The roll effect could also originate from a foot-point twisting motion as opposed to originating from the filament interaction with arcade field. This alternative is however inconsistent with Doppler observations presented in figure 12 (as well as examples 1 and 5 in table 1) and we conclude that the roll effect occurs as depicted in figure 5.

spheric/photospheric base of filament legs, as illustrated. From this perspective, the erupting filament loop also can be the reference for the observer on the positive field side of the filament. Positive roll corresponds to motion from the inside to the outside edges of the erupting filament loop. Doppler observations would reveal a gradient in the line-of-sight velocities from higher blue shifts on the inside of the loop to higher red shifted mass on the outside of the loop. Negative roll associated with dextral filaments is the opposite with blue shifts on the outside of the loops gradually reducing and changing to red shifts which become maximum on the inside of the loop. One might also remember that positive roll occurs when the top of the ribbon rolls away from the observer on the positive magnetic field side of the filament and negative roll occurs when the top of the ribbon rolls toward the observer. The erupting prominences in our observational sample exhibit a one-to-one correspondence between rolling-over direction and chirality such that positive rolling occurs for sinistral filaments

and negative rolling for dextral filaments. We give an empirical model for this in the next section.

One of the uses of establishing such a bijection is that when we observe one property, we can conclude the other without additional experimental measurements. It is true that if we see a particular filament roll in a particular direction, we can not draw a conclusion about that filament's chirality unless we also know the polarity of the photospheric magnetic field on at least one side of the filament.

Once we realized from the observations that two senses of roll existed, we suspected that a relationship to chirality might also exist. However, we had no a priori expectation as to which sign of chirality would relate to which sign of the roll effect. This came only from observations [16]. The result is shown in figure 5. In the next section we give the theoretical prediction for why the effect is as observed.

## 5 The Lorentz Force

In the treatment of filament ribbons we make the assumption that frozen-in conditions hold [17]. The frozen-in field conditions are equivalent to saying any of the following: (1) The magnetic field lines are co-moving with the fluid flow, (2) magnetic Reynolds number is effectively infinite, (3) no resistive diffusion or field line reconnection or (4) the electrical conductivity of the fluid is infinite. We would also like to emphasize that what we observe are not the field lines directly but rather plasma of different temperature than the ambient temperature. Thus the frozen-in conditions are essential to conclude that the plasma structures map the magnetic field structures.

Recall that a magnetic field line is an integral line of the magnetic field, i.e. that its direction is aligned with the field at every point. The Lorentz force  $\mathbf{F}$  is the force felt by a current  $\mathbf{J}$  due to a magnetic field  $\mathbf{B}$ ,

$$\mathbf{F} = \mathbf{J} \times \mathbf{B} \tag{1}$$

We ask what the Lorentz force upon a filament is and thus what deformation of the filament will result. As the particles *inside* the filament move along a field line, the filament exerts no discernable force upon itself; i.e. if  $\mathbf{J}$  is parallel to  $\mathbf{B}$ , then  $\mathbf{F}$  is zero. As such, we shall regard only the arcade field as powerful enough to manifest an observable deformation of the filament. Counterstreaming experiments have shown that while the velocities of the particles are indeed field-aligned, they occur in both directions with equal probability. Thus there is no velocity distinction between the two flavors of chirality [25]. Since a parity change in the magnetic field ( $\mathbf{B} \rightarrow -\mathbf{B}$ ) leaves chirality invariant (see figure 4) a structural difference between dextral and sinistral filaments is the angle that the arcade field makes with the filament. Substantial work of Helio Research has gone into the determination of these angles, the results of which will be published at a later date. The observations indicate that  $0 \leq \phi \leq 30$  for filaments in active regions,  $30 \leq \phi \leq 60$  for filaments in intermediate regions

and  $60 \leq \phi \leq 90$  for quiescent filaments (recall that  $0 \leq \phi \leq 90$  by definition from figure 4) [12]. Most, but not all, of the cases which we will list below to substantiate the roll effect are intermediate filaments.

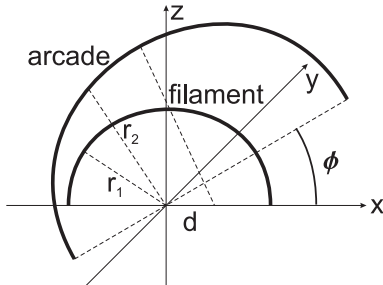


Figure 8: A schematic describing the basic features of the theoretical model and the definitions of the skew angle  $\phi$  and the spatial offset  $d$  of the filament from the arcade.

Presently, we consider a vastly simplified model which will illustrate that the force exerted by the arcade upon the filament is oppositely directed for the two flavors of chirality. Let us assume that the filament field lies in a thin flux tube with central axis  $\mathbf{f}$ . This filament rises until it hits a thin flux element in the arcade whose axis is  $\mathbf{a}$ . We assume the fields are semi-circular with radii  $r_1$  and  $r_2$  respectively. Furthermore, we assume that the arcade semi-circle is offset from the origin by  $d$  and rotated by an angle  $\phi$  (see figure 8), so that we have

$$\mathbf{f} = (x \quad 0 \quad \sqrt{r_1^2 - x^2}), \quad \mathbf{a} = (x \cos \phi \quad x \sin \phi \quad \sqrt{r_2^2 - (x+d)^2}). \quad (2)$$

with  $0 \leq x \leq r_1$ ,  $r_1 < r_2$  and  $|d| < r_1$ . The magnetic field in both field and filament will be proportional to the tangent vectors to the curves  $\mathbf{f}(x)$  and  $\mathbf{a}(x)$ . Since we are only interested in the direction of the force, we will let the constant of proportionality be unity. From this we may compute the variation in the magnetic field

$$\partial \mathbf{B} = \frac{d\mathbf{a}}{dx} - \frac{d\mathbf{f}}{dx} = \begin{pmatrix} \cos \phi - 1 \\ \sin \phi \\ \frac{x}{\sqrt{r_1^2 - x^2}} - \frac{x+d}{\sqrt{r_2^2 - (x+d)^2}} \end{pmatrix} \quad (3)$$

Let  $\mathbf{n}$  be a unit vector perpendicular to the boundary between the filament and the arcade, then the current is

$$\mathbf{J} = \mathbf{n} \times \partial \mathbf{B} \quad (4)$$

and the force

$$\mathbf{F} = \mathbf{J} \times \partial \mathbf{B} = \mathbf{n} \times \partial \mathbf{B} \times \partial \mathbf{B} \quad (5)$$

The filament has its highest point at  $x = 0$  and there the force will be strongest as there the filament will be closest to the arcade. At the point of strongest interaction, the radii of the two structures are also comparable and so we will set them equal. We evaluate the  $\mathbf{j}$  component of the force at this point to obtain (note that there are just the two cases  $d > 0$  and  $d < 0$  as  $0 \leq \phi \leq 90$ )

$$\mathbf{F}_j \approx -\frac{d \sin \theta}{\sqrt{r_2 - d^2}} \quad (6)$$

As the top of the filament is deflected by this force and the bottom continues to rise, we observe that the plane of the ribbon is tilted in the direction of  $\mathbf{F}_j$  and thus the filament obeys the roll effect.

As discussed above, the observed roll effect manifests itself through the opposite sign of the  $j$ -component of the Lorentz force of equation 6 for the two flavors of chirality. From equation 6, it is easily seen that this can only happen if  $d$  takes oppositely signed values for the two chiralities. Even though this model oversimplifies the situation, it is nevertheless characteristic in the sense that if the arcade is symmetric over the filament, no structured roll effect is possible. This interaction between observation and theory drives us to predict that there is a spatial skew (in addition to the well-known angular skew) of the arcade field with respect to the polarity inversion line over which the filament resides. Which chirality has which skew, the theory can not determine but will be told by observation.

What we can say is that if an arcade is skewed with  $d > 0$ , the force  $F < 0$  and thus, in the way we have defined it, we would obtain a negative roll; a roll against the arcade field. This simple model therefore predicts *negatively rolling filaments to have positive spatially skewed arcades above them and vice versa*. To anticipate the observations about to be discussed below, the result is that dextral filaments roll negatively and thus, according to this model have positively translated arcades ( $d > 0$ ) and vice versa. One may easily see (see figure 4 and perform the skew) that if the arcade is positively spatially skewed, the roll of the rising filament is negative, i.e. oppositely directed to the arcade field. This is exactly what the observations will tell us below.

Having accepted that the roll of dextral and sinistral (otherwise identical) filaments must be oppositely directed, one asks how one might observe this as a field parity change maintains chirality. First, we must argue that the force is independent of a field parity change. This is obvious from the definition of the Lorentz force in equation 1. Second, we observe that if a global coordinate system is defined (which of course does not change under a field parity change), then we can make comparisons. Practically this would take the form of forcing one particular cardinal direction to face the observer on any two-dimensional picture of the corona.

## 6 Observational Verification of the Roll Effect

Evidence of the roll effect during erupting prominences has been found to date in five types of solar data (1)  $H\alpha$  spectra, (2) vortical motions at the photosphere, (3)  $304\text{\AA}$  images and movies by the EIT experiment on the Solar and Heliospheric Observatory (SOHO), (4) movies at  $195\text{\AA}$  from the TRACE satellite and (5) in multi-wavelength images around  $H\alpha$  recorded at Helio Research. In Table 1 we list an outstanding example for each type of data spanning from the earliest known to us to the current year.

Rotational motion in opposite senses in the legs of erupting prominences is definitive evidence of the roll effect whether or not the speed of rotation is the same in the two legs. To differentiate rolling motion from other types of motion, such as counterstreaming, a gradient in the motion should be observed with the largest velocities of opposite sign on the outer and inner edges of the prominence. As there are many other types of motion possible in erupting prominences in addition to rolling motion, we only require that this distinctive pattern of velocities and velocity gradients be observed in major parts of the prominence for an example to be considered as having definitive evidence of the roll effect. This requirement is met for examples 1 and 5 in Table 1. See also [16].

Example 2 in Table 1 is one of five examples of vortical motions at the photosphere as found by Keil and Balasubramaniam and co-authors [6, 3, 7] at the feet of erupting prominences and near associated solar flares. Evidence for the roll effect is vortical motion similar in scale to that observed in prominence legs in other cases, location at the feet of the erupting prominence, and occurrence only during the erupting prominence. The beginning of the vortical motion as given by Keil, Balasubramaniam and co-authors is within one hour of the start of an associated flare and continuing during the rise of the flare. While small-scale vortical motions are known to be generated at the photosphere independent of the roll effect, it is not likely that vortical motion of similar scale, uniquely located at the feet of erupting prominences, and only occurring within an hour before and during the eruption would be completely independent of a concurrent erupting prominence. Therefore, we count these examples as substantial indirect evidence of the roll effect.

EIT movies at  $304\text{\AA}$  and TRACE movies at  $195\text{\AA}$  have the advantage over  $H\alpha$  and other ground-based observations of revealing more of the entire structure of erupting prominences. If the approximate motion of the mass in the legs of an erupting prominence can be tracked as it moves outward during the eruption, it is then possible in some cases to determine without ambiguity whether rotational components of motion in the legs of the eruptive are either left helical or right helical. Example 3 in Table 1 is such a case observed on 6 March 1999. In figure 9 we include 8 frames from this event observed at a 12 minute cadence in  $304\text{\AA}$  by the EIT on SOHO. We have noted from the movie that the left leg has right helical motion and the right leg has left helical motion. The rates of motion in the two legs are similar with about one turn of 360 degrees or less in each. In following the eruption site onto the disk, we identified the polarity

Table 1: OUTSTANDING EXAMPLES OF THE ROLL EFFECT IN ERUPTING PROMINENCES

	Date	Type of Data	Source of Data	Evidence of the roll
1.	1947	H $\alpha$ Spectra M.A. Ellison	Mt. Wilson Obs.	Velocity pattern with opposite directions of rotation in legs
2.	1998 Apr 7	Vortical motions at the photosphere	NSO/Sac. Peak Obs. Balasubramaniam et al. 1994	Vortical motions at photospheric feet of an erupting prominence
3.	1999 Mar. 6	304Å images	EIT/SOHO satellite (figure 9)	Opposite sense of twist in legs; form consistent with rolling
4.	1999 Oct 20	195Å images in movie format	TRACE satellite (figure 10)	Opposite sense of twist in legs; rolling at top: outside to inside
5.	2002 Jul 29	Movies in range: H $\alpha$ +/- 1.0Å	Helio Research La Crescenta, CA (see figures 10, 11, 12)	Red shifts high in prominence; blue shifts low in prominence; intermediate velocities in between; vortical motion

boundary associated with this filament and found that the west and near side of the filament was the positive polarity side as seen in magnetograms from NSO/Kitt Peak. By 7 March another filament had begun to form in the filament channel above that polarity boundary. It was intermediate between an active region filament and a quiescent filament. It was clearly seen as having dextral barbs in the daily  $H\alpha$  images from Big Bear Solar Observatory by 10 March. By the chirality rules, the channel and the erupting filament on 6 March were deduced to be dextral because dextral filaments always form in dextral filament channels. Comparing the overall form of the eruptive and direction of rotation in its legs, with the illustration in figure 5, we see that this erupting prominence is consistent with outward roll at the top of the prominence, rotational motion from the outside of the loop to the inside of the erupting loop. Therefore it has the rolling motion and eruptive form expected of dextral filaments.

Example 4 is an erupting filament observed against the disk by the TRACE satellite. The structure of the filament in the TRACE images and corresponding  $H\alpha$  images from the Big Bear Solar Observatory show it to be a sinistral filament in the southern hemisphere. As seen in figure 10, the view of the southward directed eruptive is from the positive magnetic field and equatorward side of the filament. The roll at the top is toward the south and from the inside of the erupting filament loop to the outside at the top and in both legs. Comparing these characteristics with the two types in figure 10, we find that it matches the form expected for sinistral filaments.

Example 5 is an erupting prominence observed in multi-wavelength sets of images around the  $H\alpha$  line at Helio Research on 2002 July 29. Two exposures were taken at each of nine wavelengths near  $H\alpha$ . One exposure was for revealing the  $H\alpha$  structure of the chromosphere; the other overexposed the disk to better reveal the prominence. Only the latter exposures are shown in illustrations in this paper. Prior to reaching the south west limb, the prominence was observed as a filament against the disk with sinistral barbs but here we show only the eruptive phase. A sample set of the original gray scale, multi-wavelength images in the early or pre-eruptive stage are shown in figure 10. In figure 10 the disk is intentionally overexposed to reveal more of the erupting prominence than seen than in alternate shorter exposures which show the  $H\alpha$  structure on the disk. figure 11 shows the same set of images as in figure 10 but each image is selectively color-coded to represent its Doppler shift with respect to the center of the  $H\alpha$  line. In the top row, blue, blue-green, and green colors represent increasing wavelengths respectively but all shorter in wavelength than  $H\alpha$ . These colors therefore depict all motions toward the observer. Orange, red and brown represent equivalent and increasing wavelengths longer than  $H\alpha$  and therefore all motions away from the observer. Yellow (not used in this figure) is reserved for the centerline images shown in the left column of figure 12.

The data in table 1 comprises six events that show the roll effect. For each the chirality and roll direction was determined and found to be in accordance with the theoretical prediction. Using an null hypothesis of no correlation between roll direction and chirality, our data set negates the null hypothesis at the 5 percent significance level (using chi-squared testing). Thus we conclude that

the data presented is statistically significant and provides compelling evidence for the roll effect.

The upper right image in figure 12 is a composite of all six color images in figure 11. The other two images in the right column of figure 12 are composites similarly made for two later times during the eruption. It is seen in the early stage of the eruption in figures 10, 11, and 12 that the larger red shifts during the eruption are at the top of the filament and the larger blue shifts are at the lower edge of the erupting prominence where it appears to be detaching from the chromosphere. As discussed above, this overall pattern of motions including intermediate velocities between the two extremes, is consistent with rolling motion. In this case, the top of the prominence is moving away from the observer as expected for sinistral prominences. As the eruption progresses, the rolling motion continues but stretches asymmetrically into a column above the right end of the filament such that the highest red shifts are on the right side and the highest blue shifts are more on the left side; intermediate Doppler shifts continue to form a relatively smooth gradient of velocities between these two extremes with only minor deviations from the overall pattern of roll. The rolling motion continued as the event gradually became fainter with increasing height and disappeared.

The EIT, TRACE and Helio Research examples in Table 1, are included in Table 2 along with additional examples from EIT in which there is sufficient information available to confidently establish the type of roll. The sense of roll was established in the same manner as described for the outstanding events in Table 1. Some sequences and combinations of images allow one to deduce which parts of the EIT erupting prominence structure are in front of or in back of other parts of the prominence structure as in the method described by [5]. This larger sample in Table 2 is divided according to dextral and sinistral filaments. In all examples analyzed to date, we find that dextral filaments exhibit negative roll and sinistral filaments, positive roll where positive roll is defined to be the component of motion in common the overlying coronal magnetic field. In other words, dextral filaments exhibit blue shift on the outside of the legs and red shift on the inside as in figure 10. Sinistral filaments show the reverse as in figure 11 with red shift on the outer edges and blue shift on the interior.

Relative to the outer and inner edges of the loop of the erupting filament observed from the side of the filament where the photospheric magnetic field is dominantly positive, dextral filaments exhibit outside to inside roll and sinistral filaments inside to outside roll.

Many observations of erupting prominence mass lack sufficient information to unambiguously determine whether the roll effect is taking place. Sometimes the sheet-like form is not clear and no twist is seen or an event is too complex to decipher the sense of twist. In other cases, there is too little information to distinguish front and back structures relative to the observer. In yet other cases, there might not be adequate magnetograms to determine the polarity on the two sides of the prominence. Lastly, there is not always sufficient  $H\alpha$ , He I or He II images of high enough quality to determine whether a filament or filament channel is sinistral or dextral. Nevertheless, Table 3 is only a beginning in our

Table 2: RELATIONSHIP OF THE ROLL EFFECT TO CHIRALITY

Date	Time	Sources for Roll/Chirality/Mag.	Roll Type and Direction (+ side)	Chirality
2002 Sep 26	07:19	EIT 304Å/BBSO/NSO:KP	negative outside to inside	dextral
2000 Dec 24	20:36	EIT 304Å/BBSO/NSO:KP	negative outside to inside	dextral
1999 Mar 6	12:27	EIT 304Å/BBSO/NSO:KP	negative outside to inside	dextral
2002 Sep 25	13:19	EIT 304Å/BBSO/NSO:KP	positive inside to outside	sinistral
2002 Jul 29	23:00	Helio Res./BBSO NSO:KP	positive inside to outside	sinistral
2000 Mar 24	23:04	EIT 304Å/BBSO/NSO:KP	positive inside to outside	sinistral
1999 Oct 20	6:00	TRACE/Helio Res.,BBSO /NSO:KP	positive inside to outside	sinistral

compilation of a larger set of examples of this new chiral form for erupting prominences. Combinations of data from different observatories will increase the opportunities for establishing the existence of the roll effect for much larger samples in the future.

## 7 Discussion

The roll effect also allows us the possibility of deducing the dominant sign of helicity in a filament prior to the initiation of the roll effect. The nature of the roll effect is that it necessarily adds equal and opposite twist propagating away from the roll. If a prominence already had a single and dominant sign of twist distributed nearly uniformly along the prominence, the roll effect would add to that twist in one leg and tend to remove the pre-twist in the other leg. If sinistral filaments have pre-twist that is left helical twist, then the roll effect would enhance the twist in the left leg and reduce it in the right leg. Vice-versa, if the pre-twist for a sinistral filament was right helical, the roll effect would enhance the twist in the right leg and reduce it in the left leg. Thus for sinistral filaments, enhanced twist in the right leg and reduced twist in the left leg favors right-helical pre-twist and similarly for enhanced twist in the left leg. For dextral filaments, viewed from the positive field side, the same test applies with the opposite result; left helical pre-twist would favor enhanced twist in the right leg and reduced twist in the left leg; right-helical pre-twist would favor enhanced twist in the left leg and reduced twist in the right leg. Most of

the examples in Table 2 are relatively symmetric; therefore, we do not further address this topic in this paper.

## 8 Conclusions

A new form of chirality called the roll effect is shown for erupting filaments and prominences. The two chiral forms are identified as positive or negative corresponding to the direction of motion of the top and outer edges of the legs of erupting prominences in relation to the magnetic field of the overlying coronal arcade. A physical explanation is given showing how the roll effect is expected from and consistent with the Lorentz force exerted on these structures by their overlying coronal arcades. When treated as having a ribbon-like structure, the model closely resembles observed examples of erupting filaments. The theory has given rise to the prediction that dextral filaments have positively spatially skewed arcades ( $d > 0$ , see section 5 for the definition of the parameter  $d$ ) and vice versa. This predicted effect should be amenable to observation.

Evidence of the roll effect has been found in published spectra of erupting prominences, He II 304Å images from the EIT experiment on SOHO, in at least one erupting filament observed by TRACE, in chromospheric and photospheric motions observed at NSO/Sacramento Peak, and in some H $\alpha$  Doppler images recorded at Helio Research. We conclude from this research that the legs of erupting filaments can and do sometimes simultaneously reveal both clockwise and counterclockwise twist when they erupt. Dual chirality in filaments, recently been proposed by [23], is confirmed by our results. The roll effect establishes that a single filament can concurrently show right helical structure in one part and left-helical structure in another part.

A filament possibly having both right and left helical structure implies that a negative helicity filament may have both negative and positive helicity components, the sum of these components is nevertheless negative. So while this is an interesting new effect, it does not prevent the existence of a one-to-one correspondence between total filament helicity sign and chirality as is frequently claimed. It is generally agreed that this correspondence probably exists but there has been a several-year debate on which way it goes (as mentioned in the introduction). Our result provides a new method of determining the net sign of helicity if one leg of an erupting prominence is substantially more twisted than the other, with the provision that essentially all of the prominence structure is being seen. Our current sample only included one case wherein a northern hemisphere dextral filament had its left leg much more twisted than the right leg indicating that the dominant sign of helicity prior to eruption was right helical. A definitive answer from the analysis of a statistically significant number of cases is now feasible.

## 9 Acknowledgments

The authors acknowledge helpful discussions with Alexander Ruzmaikin. The contribution of PDB was partially supported by a Valerie Mysercough Prize, SFM was supported by NASA grant NAG5-5917 and MAB gratefully acknowledges funding by PPARC grant PPA/G/S/1999/00059.

## References

- [1] Antiochos, S.K., Dahlburg, R.B. and Klimchuk, J.A. (1994) *The magnetic field of solar prominences* *Astrophys. J.* **420** L41 - L44.
- [2] Bellan, P. M. (1999) *Magnetic Helicity and Relaxation: Theory* in Brown, M. R., Canfield, R. C., Pevtsov, A. A. *Magnetic Helicity in Space and Laboratory Plasmas* Geophys. Mono. Ser. 111 (AGU, Washington), 119 - 128.
- [3] Balasubramaniam, K. S., Milano, L. and Keil, K.L. (1998) *H $\alpha$  synoptic observations of flare-filament eruption complex 1997 April 6-7* ASP Conf. Series **140** 189 - 105.
- [4] Berger, M.A. (1998): *Magnetic Helicity and Filaments.* in Webb, D., Rust, D. and Schmieder, B. (1998): *New Perspectives on Solar Prominences.* (IAU Colloquium 167, Ast. Soc. Pac., San Fransisco) 102 - 110.
- [5] Chae, J. (2000) *The magnetic helicity sign of filament chirality* *Astrophys. J.* **540** L115 - L118.
- [6] Keil, K.L., Balasubramaniam, K.S., Bernasconi, P., Smaldon, L.A., and Caussi, G. (1994) *Observations of active region dynamics: Preflare flows and field observations* ASP Conf. Series **68** 265 - 282.
- [7] Keil, S.L., Balasubramaniam, K.S., Milano, L., Bayless, A., Jones, J. and Clark, J. (1999) *Dynamical motions as precursors to activity* ASP Conf. Series **183** 540 - 550.
- [8] Low, B. C. (1996) *Solar activity and the corona* *Solar Phys.* **167** 217.
- [9] Low, B.C. and Hundhausen, J. R. (1995) *Magnetostatic structure of the solar corona 2: The magnetic topology of quiescent prominences* *Astrophys. J.* **443** 818 - 836.
- [10] Martin, S.F., Bilimoria, R. and Tracadas, P.W. (1994) *Magnetic field configurations basic to filaments and filament channels* in Rutten, R.J. and Schrijver, C.J. (ed. by) *Solar Surface Magnetism* (Kluwer Acad. Publ., Dordrecht) 303 - 338.

- [11] Martin, S.F. and Echols, C.R. (1994) *An observational and conceptual model of the magnetic field of a filament* in Rutten, R.J. and Schrijver, C.J. (ed. by) *Solar Surface Magnetism* (Kluwer Acad. Publ., Dordrecht) 339 - 346.
- [12] Martin, S.F. and A. H. McAllister (1996) *The skew of x-ray coronal loops overlying Ha filaments* in Y. Uchida, H. Hudson, and T. Kosugi (ed. by) *Magnetohydrodynamic Phenomena in the Solar Atmosphere, Prototypes of Stellar Magnetic Activity* (IAU Colloquium 153, Kluwer Acad. Publ., Dordrecht) 497 - 498.
- [13] Martin, S.F., McAllister, A.H. (1997) *Predicting the sign of magnetic helicity in erupting filaments and coronal mass ejections, in coronal mass ejections* in Crooker, N., Joselyn, J.A. and Feynman, J. (ed. by) *Geophysical Monograph 99*, AGU 127 - 138.
- [14] Martin, S.F. (1998) *Filament Chirality: A link between fine-scale and global patterns* in Webb, D., Rust, D.M., Schmieder, B. *New Perspectives on Solar Prominences* (Kluwer Acad. Pub., Dordrecht) 419-429.
- [15] Martin, S.F. (1998) *Conditions for the Formation and Maintenance of Filaments* *Solar Phys.* 182,107 - 137.
- [16] Martin, S.F. (2003) *Signs of Helicity in Solar Prominences and Related Features*. *Adv. Space Res.* **32**, 1883 - 1893.
- [17] Moffatt, H. K. (1978) *Magnetic Field Generation in Electrically Conducting Fluids* (Cambridge Uni. Press, Cambridge)
- [18] Priest, E. R. (1990) *The Equilibrium of Magnetic Flux Ropes* in Russell, C. T., Priest, E. R., Lee, L. C. *Physics of Magnetic Flux Ropes* Geophys. Mono. Ser. 58 (AGU, Washington), 1 - 22.
- [19] Priest, E.R. (1996) *New Paradigms for Solar Prominences* in Balasubramaniam, K., Keil, S., Smartt, R. (ed. by) *Solar Drivers of Interplanetary and Terrestrial Disturbances* (ASP Conf. Series) 229-241.
- [20] Priest, E.R., Hood, A.W. and Anzer, U. (1989) *A twisted flux-tube model for solar prominences. I. General Properties* *Astrophys J.* **344** 1010 - 1025.
- [21] Rust, D. M. (1999) *Magnetic helicity in solar filaments and coronal mass ejections* *Geophys. Monograph 111*, 221 - 227.
- [22] Rust, D.M. and Kumar, A. (1994) *Solar Phys.*155, 69 -
- [23] Ruzmaikin, A., Martin, S.F. and Hu, Q. (2002) *Distribution of magnetic helicity in coronal mass ejections and erupting Prominences* *J. Geophys. Res.* submitted.
- [24] Wang, Y-M. (2002) *On the relationship between HeII l304 prominences and the photospheric magnetic field* *Astrophys. J.* **560** 456 - 465.

- [25] Zirker, Engvold and Martin (1998) *Counterstreaming gas flows in solar prominences* Nature **396**, 440 - 441.

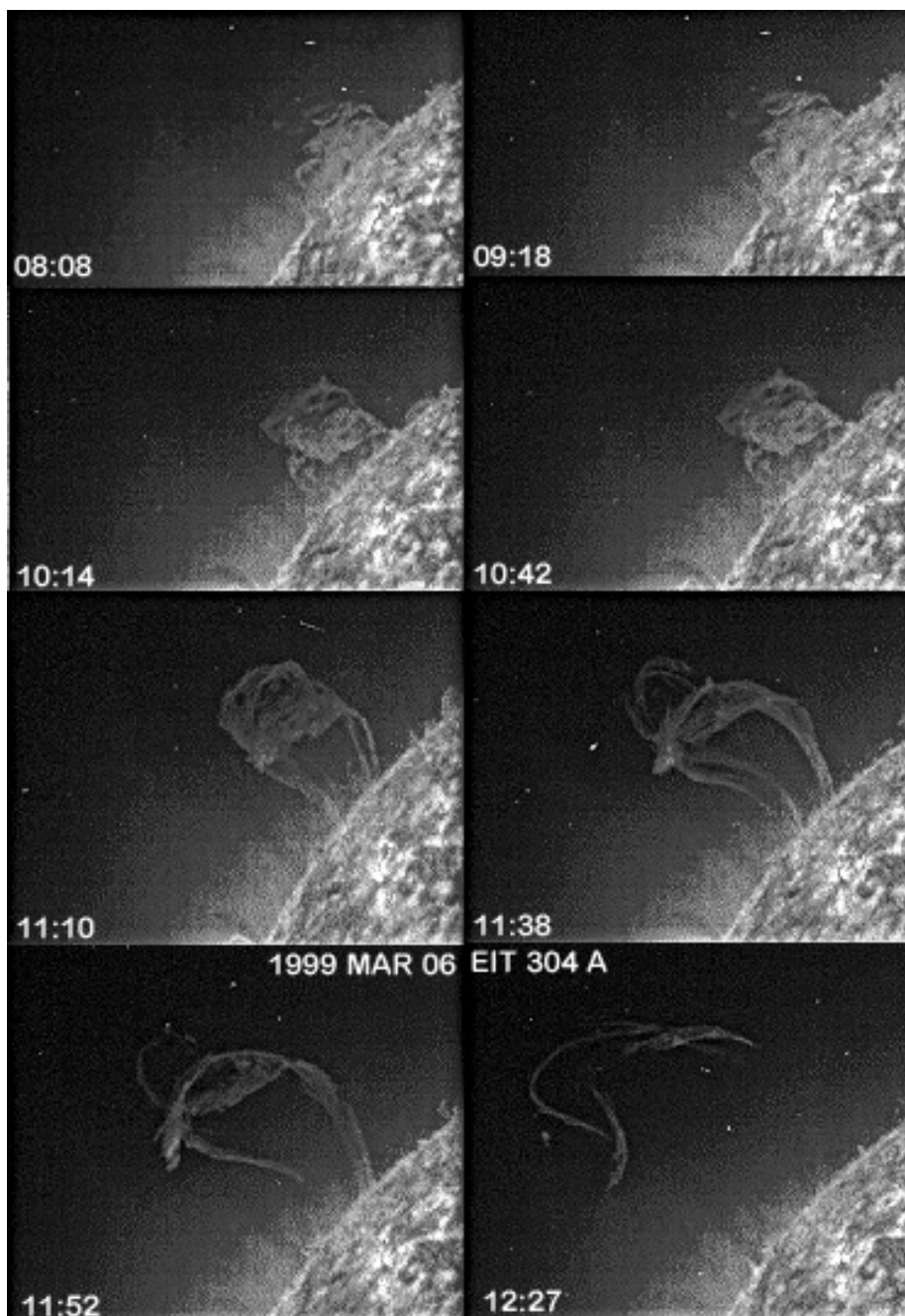


Figure 9: The March 6, 1999 event mentioned in table 1.

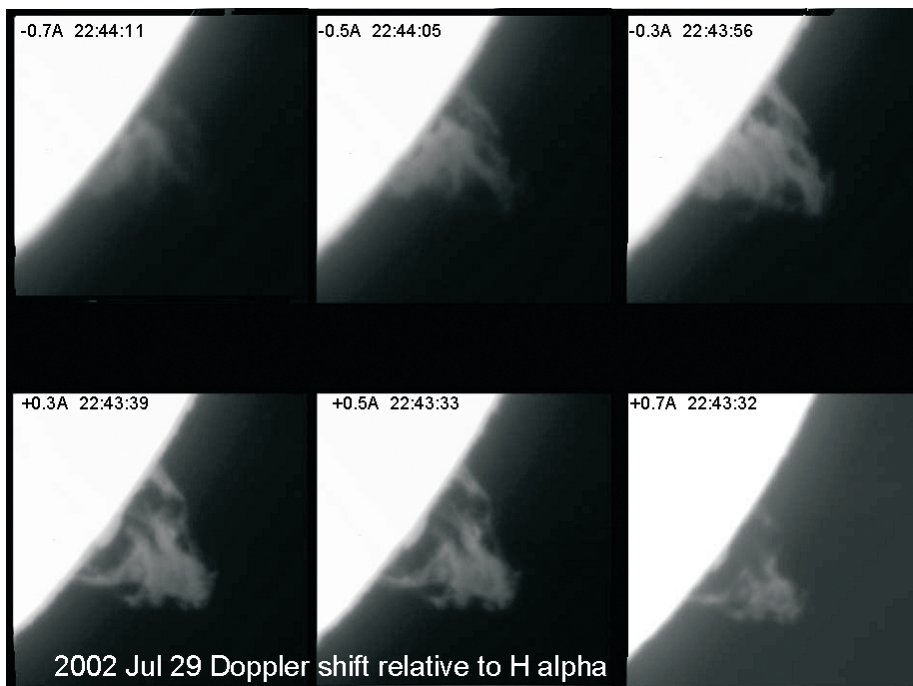


Figure 10: Panel of 6 originals - 29 Jul 2002

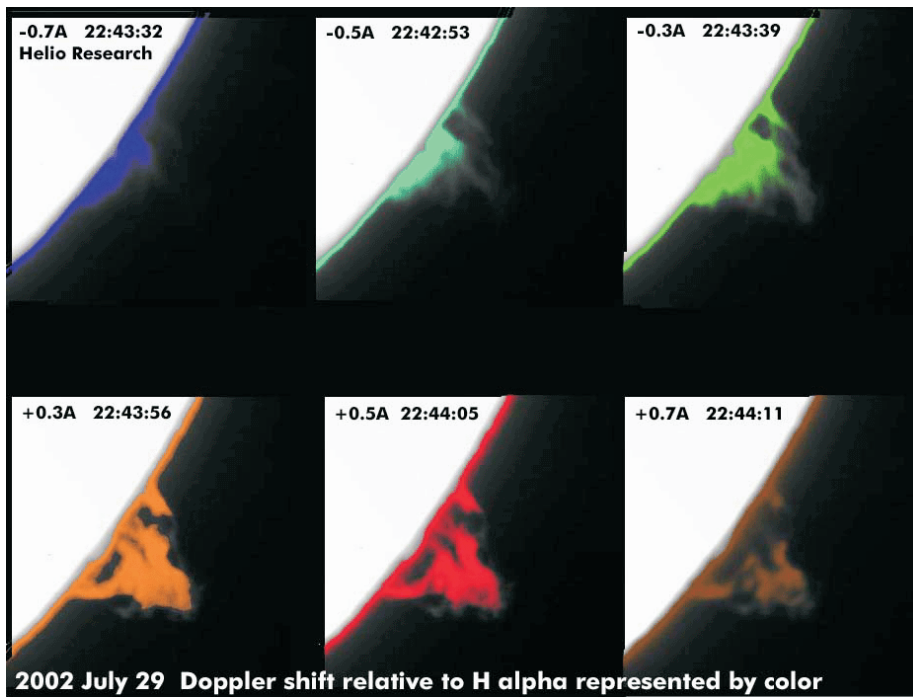


Figure 11: 6 panel colored - but otherwise as above

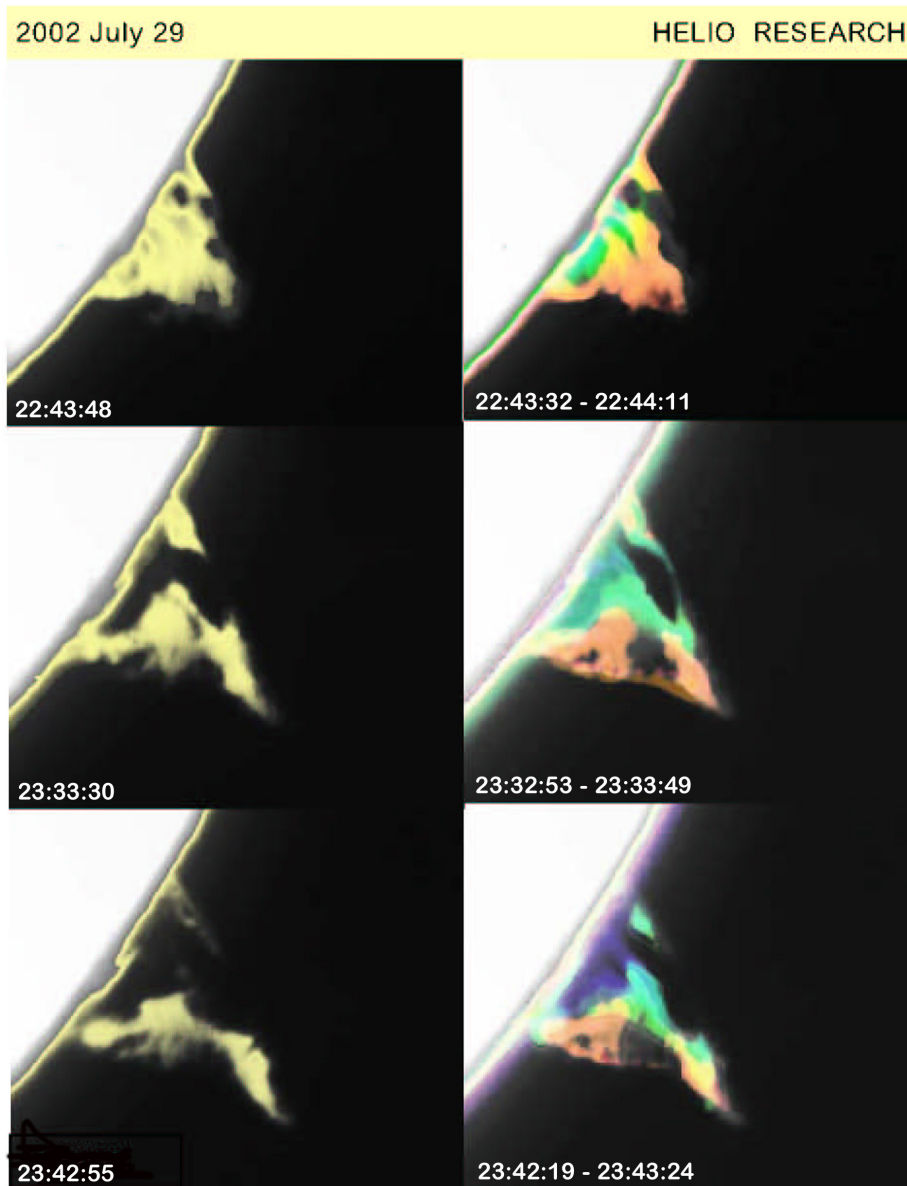


Figure 12: Multi-wavelength eruptive - 29 July 2002